Technical Note: Rapid multi-exponential curve fitting algorithm for voxel-based targeted radionuclide dosimetry

Key words: Radionuclide dosimetry, pharmacokinetics, image processing

Price Jackson[1,2]

Lachlan McIntosh[1]

Michael S. Hofman[1,2]

Grace Kong[1,2]

Rodney J. Hicks[1,2]

[1]Department of Molecular Imaging & Therapeutic Nuclear Medicine, Peter MacCallum Cancer Centre, Melbourne, Australia 3000

[2]Sir Peter MacCallum Department of Oncology, University of Melbourne, Melbourne, Australia 3010

Corresponding Author: Price Jackson

Email: price.jackson@petermac.org

Address: Dept of Physical Sciences, 305 Grattan St, Melbourne VIC, 3000, Australia

Short Title: Tri-exponential kinetics Algorithm

Abstract:

Background: Dosimetry in nuclear medicine often relies on estimating pharmacokinetics based on sparse temporal data. As analysis methods move toward image-based 3-dimensional computation, it becomes important to interpolate and extrapolate these data without requiring manual intervention; that is, in a manner that is highly efficient and reproducible. Iterative least-squares solvers are poorly suited to this task because of the computational overhead and potential to optimise to local minima without applying tight constraints at the outset.

Methodology: This work describes a fully-analytical method for solving three-phase exponential time-activity curves based on three measured time points in a manner that may be readily employed by

image-based dosimetry tools. The methodology uses a series of conditional statements and a piecewise approach for solving exponential slope directly through measured values in most instances. The proposed algorithm is tested against a purpose-designed iterative fitting technique and linear piecewise method followed by single exponential in a cohort of 10 patients receiving ^{177}Lu-DOTA-Octreotate therapy.

Results: Tri-exponential time-integrated values are shown to be comparable to previously-published methods with an average difference between organs when computed at the voxel level of 9.8±14.2% and -3.6±10.4% compared to iterative and interpolated methods, respectively. Of the three methods, the proposed tri-exponential algorithm was most consistent when regional time-integrated activity was evaluated at both voxel- and whole-organ levels. For whole-body SPECT imaging, it is possible to compute 3D time-integrated activity maps in less than 5 minutes processing time. Further, the technique is able to predictably and reproducibly handle artefactual measurements due to noise or spatial misalignment over multiple image times.

Conclusions: An efficient, analytical algorithm for solving multi-phase exponential pharmacokinetics is reported. The method may be readily incorporated into voxel-dose routines by combining with widely available image registration and radiation transport tools.

Keywords: radionuclide dosimetry, pharmacokinetics, image processing

Main Text:

Background:

Driven by increasing recognition of the clinical benefits of radionuclide therapy, particularly in neuroendocrine tumors and prostate cancer[1,2], image-based dosimetry in nuclear medicine has been a focus of physics and computational development. The MIRD committee has published coefficients for estimating radiation transport from sources at the voxel level[3] and other groups have supplemented these tables for a variety of cubic dimensions and common therapeutic isotopes[4,5]. This has been extended to patient-specific Monte Carlo calculations, which may now be performed in a clinically-achievable timeframe[6,7]. There has been consideration of the spatial effects of ionisation relative to source location with respect to the resolution of the imaging systems used to infer that source distribution[8]. There has also been work extending dose metrics to infer radiobiological effect according to dose-rate and spatial heterogeneity[9].

While much focus has been applied to computation of radiation physics, research in pharmacokinetic interpolation is relatively limited. Inferring the input time-integrated activity map—a 3-dimensional grid of the number of disintegrations per voxel—represents a comparably challenging task both in terms of complexity and potential to introduce errors in the predicted dose-volume. In the ideal instance, this is performed entirely in the image space allowing dosimetry to be appreciated at the level of detail attained by a SPECT imaging system. Typically, this workflow involves serial acquisition of multiple quantitative SPECT images[10] with pharmacokinetic time-activity curves (TACs) derived independently for each position in the aligned image sequence[11].

One of the primary challenges in computing voxelized TACs is employing a routine that is generalizable—that is, one that can be applied uniformly throughout the variety of tissues in the body—while operating without manual oversight and at minimal concession to fitting accuracy. Sarrut *et al.* described an algorithm that places voxels into different classes to simplify the optimisation challenge and penalise models based on their complexity[12]. This, in principle, yields more reproducible results than an unconstrained least-squares method. A similar approach had previously been employed by Kletting *et al.* to enable users to designate between a variety of fitting functions based on the shape of pharmacokinetic measurements, however, in requiring user input would not be appropriate for voxel level dose estimation[13]. In this work a general three-phase exponential model is applied which offers the flexibility to characterise components of uptake as well as a mixture of slow and fast tissue clearance components.

An analytical pharmacokinetic estimation technique is reported in detail including the sequence of computational operations and methods for handling noisy or otherwise irregular data. The technique provides the basis for a previously-published voxel dosimetry software package[14] and has been shown to be reliable across a variety of clinical trial datasets[15]. Given that all phases of the pharmacokinetic curves—even those of uptake—may be described by equations of exponential decay, it is possible to approach the problem as a piecewise operation. By solving for the slope between the final two measurements, the preceding phases can be solved in sequence moving to earlier times based on the difference between measured values and the trajectory of the previously predicted phase as a simplified curve-stripping process[16]. Depending on the data conditions, where measurement values lie within respective reference lines, the most appropriate order of solving may vary. In some instances, for example when activity continues to increase beyond the second image time, the curve is best approximated by only two phases using sustained uptake from injection to the final measurement, followed by physical decay in the period beyond. This facilitates simplification of a highly unconstrained problem—six variables with only three data points—using only a few straightforward assumptions and computational logic operations. With judicious selection of acquisition times, this form of curve generation may be applied in a manner that is representative, and without systematic bias, for a wide variety of pharmacokinetic models.

Methods:

With the aim to solve parameters that define a three-phase exponential curve described by Equation 1, $A_{1\text{-}3}/k_{1\text{-}3}$, the ideal case includes a single phase of tissue uptake and up to two phases of clearance.

This model may describe periods of rapid washout and long-term retention; each with a variable half-life and relative proportion as represented across a variety of pharmacokinetic tissue types.

$$\boldsymbol{Region\ Activity} = \boldsymbol{A_1 e^{k_1 t} + A_2 e^{k_2 t} + A_3 e^{k_3 t}}$$

Equation 1

[Figure 1]

Three activity concentration values are described as $c_{1\text{-}3}$ and time points as $t_{1\text{-}3}$. As a preliminary step, the convention is taken to decay-correct all image data, $c_{i1\text{-}3} \rightarrow c_{1\text{-}3}$, as illustrated in Figure 1. This handles concentration values in pharmacological terms during fitting. The decay-correction is straightforward to reverse when taking the final integral calculation and offers practical advantage to ensure that the pharmacological concentration does not continue to increase beyond the final imaging time point. This should be a reasonable assumption given judicious selection of imaging time points[17]. Specifically, it prevents the final integral from exceeding a value that would exceed the physical half-life of the isotope; curves which deplete more slowly than the half-life of the radionuclide. If the highest activity measurement is detected at the final time point, fitting a slope very near zero, $k_3 \approx -\infty$, equates to only physical decay. Secondly, this provides a simple mechanism to adapt the algorithm for other isotope or diagnostic/therapeutic pairs, for example using sequential ^{124}I PET/CT imaging to predict radiation dose from ^{131}I radioactive iodine. The user only needs to provide the physical half-life of each tracer and the same algorithm may be applied to compute local time-integrated activity concentration (decays per unit volume) for the given quantity of activity administered.

[Figure 2]

The ideal case can be described by a transient uptake phase between t=0 and t_1 followed by distinct periods of rapid and delayed washout in the $t_{1\rightarrow 2}$ and $t_{2\rightarrow 3}$ time spans, respectively, as shown in Figure 2. In clinical use of long half-life therapeutic isotopes, after initial uptake, one or two exponential clearance phases of activity from organs and tumors are widely described[18]. It is possible to fit a curve of exponential decay between two points as shown in Figure 3 with the form:

$$A = A_0 e^{kt}$$

Equation 2

Solving for the linear fit, $y = mx + b$, by log transform of the activity values starting with the final phase, the kinetic parameter, k_3, is determined by:

$$k_3 = m = \frac{\ln(c_3) - \ln(c_2)}{t_3 - t_2}$$

Equation 3:

And the amplitude parameter, A_3, is then:

$$A_3 = e^b = e^{\ln(c_2) - k_3 t_2}$$

Equation 4:

[Figure 3]

As a first instance, this method provides the slope of the line representing the long-term retention phase. The preceding phase can be described as the difference between the slope described by the A_3,k_3 curve and the value at c_1 using another exponential decay equation that depletes as it approaches t_2. This very nearly builds a piecewise function from exponential terms. Solving by log transform requires non-zero values, so, for simplicity, we adjust the latter activity value, delta c_2, to be in the range of 1-3% of the measured value c_2. Some discussion of the special conditions which warrant the variability is provided in later sections. The process may be more clearly illustrated by the mixture of curves in Figure 4. The residual of the curve, Δc_1, is the difference between the slope of the late phase and the first measured activity value, c_1:

$$\Delta c_1 = c_1 - A_3 e^{k_3 t_1}$$

Equation 5:

The sign of the delta value is evaluated: $\Delta c_2 = 0.01 * c_2$ if Δc_1 is greater than zero. If not, the sign is reversed to $\Delta c_2 = -0.01 * c_2$. That is, both delta values should be positive or negative. There are conditions when a negative A_2 provides the most appropriate fit based on the measured data. Curve approximation then follows the previous method of solving for exponential slope to generate a phase that depletes as it approaches c_2:

$$k_2 = \frac{\ln(\Delta c_2) - \ln(\Delta c_1)}{t_2 - t_1}$$

$$A_2 = e^{\ln(\Delta c_1) - k_2 t_1}$$

Equation 6:

[Figure 4]

Estimating the very early uptake kinetics requires an approximation when there are no intermediate points before the peak activity measurement. This is typical when only one image is available during the first day of administration. One approach is to infer the uptake pharmacokinetics based on a generic rate constant, k_1. For long half-life therapeutic isotopes, the majority of the time-integrated activity calculation is dictated by the late-phase retention. That is, if the physical half-life is several days or longer, only select tissues with significant initial uptake followed by rapid and sustained clearance could be appreciably impacted by the use of a generic uptake parameter. The notable exception is choosing a very small k_1 parameter representing very rapid uptake. In this case, the presented algorithm may yield a curve that escalates dramatically at times close to t=0 due to the nature of solving the line-of-fit for the fast clearance phase. With ^{177}Lu, a half-time of approximately 30 minutes, k_1=-1.3, has been shown to offer reasonable agreement with other curve-fitting integrals over a range of different tissue types[14,19]. An analysis of the influence of the generic rate parameter on time-integrated activity is provided in Supplementary Table 1 showing that over a range of half-times from 20 to 90 minutes, the effect is in the order of ±2% except in bladder and heart (blood pool). Finally, the amplitude, A_1, of the uptake phase is set such that concentration value passes through zero at t=0. Here the term A_1 becomes the negative of the sum of A_2 and A_3.

In this manner, it is possible to analytically solve a three-phase exponential that very closely passes through three measured time points. This piecewise method, or a slightly modified version, can be applied wherever declining slope is detected between values of c_2 and c_3; that is, whenever some clearance is detected in the late phase of imaging as would be typical of most tracers and tissue types. The sequence of computations is depicted in the flowchart shown by Supplementary Figure 6 with this common case designated by bold labels.

With the solved time-activity curve, it is then possible to integrate the decay-corrected curve from $t_{0\rightarrow inf}$ including the physical half-life of the isotope in the form:

$$\tilde{A} = \frac{A_1}{(\frac{ln2}{t_{1/2}} + k_1)} + \frac{A_2}{(\frac{ln2}{t_{1/2}} + k_2)} + \frac{A_3}{(\frac{ln2}{t_{1/2}} + k_3)}$$

Equation 7:

Where $\tilde{A}$ is the time-integrated activity or total number of disintegrations in the region described by the time-activity curve, $t_{1/2}$ is the physical half-life of the therapeutic isotope, and the parameters $A_{1\text{-}3}$ and $k_{1\text{-}3}$ are the fitting values described previously.

A detailed explanation of conditional methods to derive curves for irregular, or slowly-accumulating data is provided in the supplementary material (Supplementary Figures 1-3). This involves methods to classify the shape of the curve to apply algorithmic steps suited to that pharmacokinetic type. In some instances, such as when activity decreases from c_1 to c_2 and increases again at c_3 the algorithm will interpolate an intermediate location to analytically define a curve that balances the necessary error between measurements with a behaviour that is similar to least-squares optimisation. It is worth noting that for these cases, the convention is taken to define a curve that as often as possible passes directly through the final measurement time—typically the most important for long half-life isotopes—and subsequently mitigate the error for the line-of-fit that passes through or near the preceding times. Flow charts to illustrate the conditional sequence of processing are given in Supplementary Figures 4-6.

The multi-exponential algorithm was tested in clinical application in a representative cohort of 10 patients receiving ^{177}Lu-DOTA-Octreotate. Cases were followed-up by serial post-treatment quantitative SPECT imaging at timelines of 4, 24, & 72 hours. Pharmacokinetics were then computed at the voxel level with the proposed tri-exponential algorithm. For comparison to two reference methodologies, time-integrated activity was estimated by piecewise linear approximation between image times followed by a single exponential phase determined by the effective half-life over the final two image acquisitions[20].

In voxels where the detected clearance rate was slower than the physical half-life of ^{177}Lu, clearance was instead based on physical decay. Secondly, the iterative fitting technique described by Sarrut *et al.,* the Voxel-based Multimodal method (VoMM), was implemented with Python libraries[12,21]. In that method, iterative optimization is performed for each voxel according to four different single- or multi-exponential models and the most accurate line-of-fit with a penalty for model complexity is chosen. The resulting time-integrated activity concentration for each technique was compared both at the voxel level and based on a single curve derived from the mean activity in each volume-of-interest. For tumor and a selection of relevant tissues (kidney, spleen, liver, bladder, marrow, etc) time-integrated activity was assessed. Additionally the mean absolute error as weighted for voxel activity in predicted curves with the tri-exponential algorithm and VoMM method was investigated for each imaging time point. The median of all cases with each technique is summarized.

Results:

This work presents a computationally efficient methodology to solve highly unconstrained curve fitting in a predictable manner. The authors have previously demonstrated that this algorithm yields comparable regional dosimetry when applied independently across regional voxels to whole-organ methods employed with OLINDA coupled with a traditional iterative curve solver[14,19]. In comparison to alternative voxel methods including trapezoidal interpolation followed by a single exponential and the previously published VoMM iterative technique, closest agreement between methods was observed in long-retaining tissues. Time-integrated activity in high-uptake organs (kidney, liver, spleen)—those considered at-risk in ^{177}Lu-Ocreotate therapy—was on average within 10% for all curve fitting methods evaluated at the voxel level. Results for the 10 patient cohort are summarised in Table 1 and an evaluation of median voxel-wise fitting error at each of the three imaging time points is reported for the tri-exponential and VoMM techniques in Table 2. The three methods were observed to be in closer agreement when pharmacokinetics were computed at the organ- rather than voxel-level where the tri-exponential algorithm was within 5% of the VoMM technique for all regions except for bladder, intestines and pancreas. Of the three, the proposed tri-exponential algorithm most closely reproduces the whole organ time integrated activity result when calculated from independent voxel curves with the lowest variation observed for 8 of the 15 regions including tumor, marrow, liver, and left kidney.

In comparison to a trapezoidal interpolation followed by single-exponential model, the multi-exponential model was typically 3.5% lower in terms of estimated integral decays with most organs in the range of -1 to -8%. Much of the area under the curve for these therapies is dictated by the late phase retention which should be similar in most cases with single- and tri-exponential evaluations. A significant difference in dose to bladder is reported with all three methods which may be attributed to the relative variation in uptake between images on the first day of therapy and those acquired at 24 hours and beyond. Where tissues displaying this form of clearance are relevant for assessing potential toxicity, it is advisable to collect finer temporal sampling in the first day post-administration.

The scripted implementation of the fitting algorithm using Python computes at a rate of approximately 5,000 voxels per second with clinical image data[14,22]. Applying a condition to ignore background voxels—those with very low activity values—dose volumes for a multi-bed SPECT series at 3.0mm cubic spatial resolution can be computed in less than five minutes. Processing times were comparable to trapezoidal and single-exponential model. The iterative VoMM method was considerably more computationally intensive, previously reported at 800 voxels per second[12], however the python-based implementation would not be practical to apply across the full image space and voxel-wise fitting was restricted to labelled subregions. Image-based pharmacokinetics processing is often coupled with non-rigid image registration to tightly fuse the serial time points across the image volume[23]. That step will typically be equally or more computationally intensive than the pharmacokinetics process described in this work and as such this method of pharmacokinetic interpolation should not be considered a significant bottleneck to clinical workflows. As a complete image-based dosimetry tool, the algorithm has been employed in a variety of clinical studies for both therapeutic and diagnostic dose evaluation which have been used to inform patient management[24-27].

[Table 1]

The overall residual error was observed to be comparable between iteratively optimized and tri-exponential algorithms, however, the VoMM method was shown to be most accurate at the early image phase with increasing error at later time points. This is to be anticipated as the observed activity—and potential to influence sum of squared error—carries less weight for the optimization task. In contrast, the proposed tri-exponential algorithm is designed to fit directly through the 2nd and 3rd measurements wherever the shape of the curve would sensibly permit. This may necessarily come at the sacrifice of accuracy in the very early phases; for example, in bowel which can be slow to accumulate ^{177}Lu-Octreotate over several days.

[Table 2]

Discussion:

This work aims to describe an automated, reproducible and efficient methodology for solving a large volume of time-activity curves with application to nuclear medicine dosimetry. The choice of three-phase exponential model affords the flexibility to characterise periods of tracer uptake as well as mixtures of slow- and fast-clearance. By considering the sequence of operations, it is possible to address model over-complexity: solving the most important phase at the outset and applying additional phases as necessary with decreasing influence on the time integral. The resulting algorithm is designed to yield comparable estimates of time-integrated activity to traditional methods including linear piecewise interpolation or constrained least-squares optimisation. Additionally as a pure exponential model, it is straightforward to apply isotope decay corrections and integral calculations. Many of the standard kinetic coefficients selected in the present implementation are chosen empirically as a practical solution for use in ^{177}Lu-DOTA-octreotate dosimetry and with imaging times routinely used in clinical practice. The conditional methods have been shown to reliably approximate time-integrated activity estimates from other curve-fitting techniques when compared both at the voxel and organ level.

It has been consistently reported that delayed image acquisitions are most important to accurately estimate dosimetry in ^{177}Lu therapies even for complex pharmacokinetic models[28,29]. The algorithm in this work is designed to yield curves which pass through the final acquisition time and, where appropriate, will directly determine late phase clearance based on the line of slope between the second and third image acquisitions. This is in contrast to most iterative least-squares solvers which, in the ordinary case, will be weighted toward uptake when activity is largest, typically at the earliest time point and may be at the expense of accurately characterizing time-integrated activity. This can be improved upon by modifying the objective function to bias the weighting of certain measurements either explicitly or through additional iterative operations [30], but this presents a different set of challenges if the aim is to implement as a general purpose tool to efficiently run in the image space. Balancing patient convenience with quantitative accuracy and ease of use is a motivation for improved algorithms for clinical dosimetry.

There are intrinsic limitations to fitting a six-variable equation to three measured data points; or effectively four if directed through zero at the origin and generic uptake rates are considered. Even with well-conditioned data, the combination of clearance half-times and fractions may be modified to yield an infinite number of solutions which pass through the measurement values. This is constrained if each phase of the multi-exponential term depletes to very near zero as it transitions from one measurement to the next. Subsequently, the shape of the curve is influenced by the selection of image times as the inflection between phases 2 and 3 will necessarily occur at the second measurement time. If the time points are not chosen sensibly, or there are inconsistencies in the image times between patients within a cohort, systematic bias could result. This, however, is a challenge for any pharmacokinetic assessment methodology and it is worthwhile to restate the importance of judicious selection of measurements with consideration of the pharmacokinetics and physical half-life of any radiopharmaceutical. Of specific note, when using short half-life isotopes or imaging in the first two hours of administration, it is advisable to experiment with the standard uptake rate coefficient, k_1, which may be modified (and likely reduced) to reliably model the underlying physiology. As with the selection of uptake half-time, the use of conditional assumptions may warrant special consideration for the pharmacokinetics of individual tracers with ^{124}I, ^{131}I and ^{90}Y being of particular interest in the context of current therapeutic radionuclides. Additionally, with increasing focus on the potential for theranostic isotope pairs such as ^{86}Y/^{90}Y, ^{44}Sc/^{47}Sc, or ^{64}Cu/^{67}Cu which permit delayed, high-resolution imaging and treatment with an equivalent molecular species, the ability to assess pharmacokinetics in the image space is particularly relevant.

In this report, a working version of the algorithm is distributed as open-source software, which may be employed directly or improved upon by contributing researchers. Because the algorithm runs with a set of conditional statements and a sequence for solving for exponential slope between two points, it is possible to implement in software that handles basic conditional and mathematical operations. For demonstration or use as a region-based dosimetry tool, the algorithm has been incorporated into an interactive spreadsheet, which is available in the supplementary material supporting this article or at the primary author's Github repository[31].

Conclusions:

This report presents a generalizable algorithm to derive time-activity curves from limited temporal measurement data. The methodology relies on separating the curve-fitting challenge into piecewise phases similarly to a residual stripping technique. Conditional statements allow the process to be applied in a predictable manner that achieves a sensible compromise in error for voxels which may be subject to noise or inconsistent co-registration. The technique is computationally efficient allowing use for routine image-based dosimetry. A complete version of the algorithm is provided as open-source computer code for developers of nuclear medicine analysis software.

Acknowledgements:

PJ is supported by a Victorian Cancer Agency clinical fellowship. Initial clinical data provided through grant support by the Victorian Cancer Agency clinical trial, “GaTate-PET/CT to predict LuTate dosimetry in patients with neuroendocrine tumour disease: a pilot study” (CI RJH). MSH is supported by a Clinical Fellowship Award from the Peter MacCallum Foundation and receives grants from the Prostate Cancer Foundation (PCF), Movember, U.S. Department of Defence and the Prostate Cancer Foundation of Australia. He also receives research funding from Advanced Accelerator Applications (a Novartis company). GK is supported by a Clinical Fellowship Award from the Peter MacCallum Foundation. RJH is recipient of a National Health and Medical Research Council Practitioner Fellowship (APP1108050). The authors would like to thank David Sarrut for his advice and input in evaluating the methodology in comparison to his previously published technique.

Conflicts-of-interest:

The authors have no conflicts to disclose

Citations:

1. Fanti S, Minozzi S, Antoch G, et al. Consensus on molecular imaging and theranostics in prostate cancer. *The Lancet Oncology.* 2018;19(12):e696-e708.
2. Kwekkeboom DJ, Krenning EP, Lebtahi R, et al. ENETS consensus guidelines for the standards of care in neuroendocrine tumors: peptide receptor radionuclide therapy with radiolabeled somatostatin analogs. *Neuroendocrinology.* 2009;90(2):220-226.
3. Bolch WE, Bouchet LG, Robertson JS, et al. MIRD pamphlet no. 17: the dosimetry of nonuniform activity distributions—radionuclide S values at the voxel level. *Journal of Nuclear Medicine.* 1999;40(1):11S-36S.

4. Lanconelli N, Pacilio M, Meo SL, et al. A free database of radionuclide voxel S values for the dosimetry of nonuniform activity distributions. *Physics in Medicine & Biology.* 2012;57(2):517.

5. Dieudonné A, Hobbs RF, Bolch WE, Sgouros G, Gardin I. Fine-resolution voxel S values for constructing absorbed dose distributions at variable voxel size. *Journal of nuclear medicine.* 2010;51(10):1600-1607.

6. Pacilio M, Lanconelli N, Lo Meo S, et al. Differences among Monte Carlo codes in the calculations of voxel values for radionuclide targeted therapy and analysis of their impact on absorbed dose evaluations. *Medical physics.* 2009;36(5):1543-1552.

7. Jackson PA, Hickson K. Integration of GATE Monte Carlo-based radionuclide dosimetry as a practical on-line clinical tool. Paper presented at: 2017 Geant4 User Workshop2017; University of Wollongong, Wollongong, Australia.

8. Pacilio M, Amato E, Lanconelli N, et al. Differences in 3D dose distributions due to calculation method of voxel S-values and the influence of image blurring in SPECT. *Physics in Medicine & Biology.* 2015;60(5):1945.

9. Sgouros G, Frey E, Wahl R, He B, Prideaux A, Hobbs R. Three-dimensional imaging-based radiobiological dosimetry. Paper presented at: Seminars in nuclear medicine2008.

10. Dewaraja YK, Frey EC, Sgouros G, et al. MIRD pamphlet no. 23: quantitative SPECT for patient-specific 3-dimensional dosimetry in internal radionuclide therapy. *Journal of Nuclear Medicine.* 2012;53(8):1310-1325.

11. Ljungberg M, Celler A, Konijnenberg MW, Eckerman KF, Dewaraja YK, Sjögreen-Gleisner K. MIRD pamphlet no. 26: joint EANM/MIRD guidelines for quantitative 177Lu SPECT applied for dosimetry of radiopharmaceutical therapy. *Journal of nuclear medicine.* 2016;57(1):151-162.

12. Sarrut D, Halty A, Badel JN, Ferrer L, Bardiès M. Voxel-based multimodel fitting method for modeling time activity curves in SPECT images. *Medical physics.* 2017;44(12):6280-6288.

13. Kletting P, Schimmel S, Kestler H, et al. Molecular radiotherapy: The NUKFIT software for calculating the time-integrated activity coefficient. *Medical physics.* 2013;40(10):102504.

14. Jackson PA, Beauregard JM, Hofman MS, Kron T, Hogg A, Hicks RJ. An automated voxelized dosimetry tool for radionuclide therapy based on serial quantitative SPECT/CT imaging. *Medical physics.* 2013;40(11).

15. Violet J, Jackson P, Ferdinandus J, et al. Dosimetry of 177Lu-PSMA-617 in Metastatic Castration-Resistant Prostate Cancer: Correlations Between Pretherapeutic Imaging and Whole-Body Tumor Dosimetry with Treatment Outcomes. *Journal of Nuclear Medicine.* 2019;60(4):517-523.

16. Kirkup L, Sutherland J. Curve stripping and nonlinear fitting of polyexponential functions to data using a microcomputer. *Computers in Physics.* 1988;2(6):64-68.
17. Siegel JA, Thomas SR, Stubbs JB, et al. MIRD pamphlet no. 16: techniques for quantitative radiopharmaceutical biodistribution data acquisition and analysis for use in human radiation dose estimates. *Journal of Nuclear Medicine.* 1999;40(2):37S-61S.
18. Stabin M, Xu XG. Basic principles in the radiation dosimetry of nuclear medicine. Paper presented at: Seminars in nuclear medicine2014.
19. Stabin MG, Sparks RB, Crowe E. OLINDA/EXM: the second-generation personal computer software for internal dose assessment in nuclear medicine. *Journal of nuclear medicine.* 2005;46(6):1023-1027.
20. Grassi E, Fioroni F, Ferri V, et al. Quantitative comparison between the commercial software STRATOS® by Philips and a homemade software for voxel-dosimetry in radiopeptide therapy. *Physica Medica.* 2015;31(1):72-79.
21. Virtanen P, Gommers R, Oliphant TE, et al. SciPy 1.0: fundamental algorithms for scientific computing in Python. *Nature Methods.* 2020:1-12.
22. Van Der Walt S, Colbert SC, Varoquaux G. The NumPy array: a structure for efficient numerical computation. *Computing in Science & Engineering.* 2011;13(2):22.
23. Klein S, Staring M, Murphy K, Viergever MA, Pluim JP. Elastix: a toolbox for intensity-based medical image registration. *IEEE transactions on medical imaging.* 2010;29(1):196-205.
24. Willowson KP, Ryu H, Jackson P, Singh A, Eslick E, Bailey DL. A comparison of 2D and 3D kidney absorbed dose measures in patients receiving 177Lu-DOTATATE. *Asia Oceania Journal of Nuclear Medicine and Biology.* 2018;6(2):113.
25. Hicks RJ, Jackson P, Kong G, et al. First-in-human trial of 64Cu-SARTATE PET imaging of patients with neuroendocrine tumours demonstrates high tumor uptake and retention, potentially allowing prospective dosimetry for peptide receptor radionuclide therapy. *Journal of Nuclear Medicine.* 2018:jnumed. 118.217745.
26. Pattison DA, Solomon B, Hicks RJ. A new theranostic paradigm for advanced thyroid cancer. *Journal of Nuclear Medicine.* 2016;57(10):1493-1494.
27. Kong G, Callahan J, Hofman MS, et al. High clinical and morphologic response using 90 Y-DOTA-octreotate sequenced with 177 Lu-DOTA-octreotate induction peptide receptor chemoradionuclide therapy (PRCRT) for bulky neuroendocrine tumours. *European journal of nuclear medicine and molecular imaging.* 2017;44(3):476-489.

28. Hänscheid H, Lapa C, Buck AK, Lassmann M, Werner RA. Absorbed dose estimates from a single measurement one to three days after the administration of 177Lu-DOTATATE/-TOC. *Nuklearmedizin.* 2017;56(06):219-224.

29. Madsen MT, Menda Y, O'Dorisio TM, O'Dorisio MS. Single time point dose estimate for exponential clearance. *Medical physics.* 2018;45(5):2318-2324.

30. Muzic Jr RF, Christian BT. Evaluation of objective functions for estimation of kinetic parameters. *Medical physics.* 2006;33(2):342-353.

31. Jackson PA. Github - TriExponential-Solver. 2019; https://github.com/jacksonmedphysics/TriExponential-Solver.

Supplementary Material:

Handling of irregular data:

When performing operations across many thousands of voxels that may be prone to noise or image alignment errors, there are likely to be challenging locations that warrant special consideration to yield curves and integrals which represent fair approximations of the underlying data. In instances where the highest activity is detected at t_3, a reasonable convention is to assume that only physical decay occurs at time points beyond[20]; or for simplicity that there is very slight pharmacological clearance such that the effective half-time is determined by the physical half-life of the isotope as illustrated in Supplementary Figure 1. In the proposed method, setting k_3 to a value near zero yields an equivalent computation when applied to decay-corrected data. The coefficient A_3 may be solved according to Equation 4. There may be no need to fit multiple uptake phases in this instance (A_2=0). Instead, the method from Equation 6 is used to solve for a single uptake phase that reaches a maximum as it nears c_3. There is scope to moderate the uptake kinetics based on the measured data points c_1 and c_2, as illustrated in the flow chart shown by Supplementary Figure 5. Nevertheless, the area under the curve for long half-life isotopes will be primarily dictated by the amplitude of uptake at measurement c_3. In other instances, this type of curve may be physiologically appropriate.

[Supplementary Figure 1]

The most apparent case where the data requires correction from the outset is when the trajectory of uptake or clearance changes multiple times across the measurement points. This may occur when a region initially displays a large activity concentration that appears to decrease at the time of the second image and subsequently increases again at the third. In image-based dosimetry, these instances are often artefactual; produced due to noise or small misalignments near the margin of high-uptake tissues such as kidneys and spleen. Here, the aim is to mitigate potential errors and yield a curve that approximates the behaviour of a least-squares fitting routine. In this methodology, the convention is taken that the final time point is most important to determine the time integral. The values of the first two points are moderated such that it is possible to apply a curve solving methodology which balances error with respect to the early phase(s) as shown in Supplementary Figure 2.

[Supplementary Figure 2]

Solving exponential slope between values that transition to very near zero can be problematic. This tends to occur for voxels in low-uptake regions where small changes in absolute activity concentration represents very large relative differences if one of the values is near zero. Although this type of measurement is largely influenced by scanner sensitivity in background regions and reconstructed noise, using those rate kinetics parameters leaves the potential to infer extremely high uptake in the very early time window and, as such, overestimate time-integrated activity. As a practical fix, the relative uptake can be initially compared across time-points and adjusted if necessary—in this case c_3 is modified to 10% of the value at c_2 as shown in the preconditioning flow-chart, Supplementary Figure 4—to yield a more sensible curve and estimate of integral decays.

Additionally, computation of two threshold c_2 values are used to define the limits for the slope between the values of c_1 and c_3. The first, $c_{2,\mathrm{plateau}}$, is used to test whether activity increases between time points 2 and 3. If the activity at c_1 is also very low, as may occur in some tissues that slowly accumulate tracer such as bowel in ^{177}Lu-PMSA therapy, no correction would be warranted. In other cases where activity initially declines from c_1 to c_2 only to increase again at the final measurement such as shown in Supplementary Figure 2, it is logical to assume that some element of the measurement is artefactual. Shifting the value of c_2 up to the plateau point where the exponential fit between c_2 and c_3 achieves minimal biological clearance; or effectively only physical decay from t_2 and passing through the measurement c_3. With this parameter solved, it is then possible to apply the piecewise methodology to solve the remaining phases that may appropriately to pass through c_1.

[Supplementary Figure 3]

When the concentration at c_2 appears as less than a linear interpolation between time points c_1 and c_3 (illustrated in Supplementary Figure 3), a solution is to compute a value that falls on that line, $c_{2,linear}$, that may replace the original value if increasing slope is required to approximate the curve up to the final imaging time. The resulting curve is illustrated in Supplementary Figure 3 and the implementation into the algorithmic workflow can be traced in Supplementary Figure 5 and Supplementary Figure 6.

[Supplementary Figure 4]

[Supplementary Figure 5]

[Supplementary Figure 6]

Selection of Generic Uptake Rate Parameter (k_1):

For the common condition where fast- and slow-clearance components are observed it is sensible to implement a generic uptake rate in order to prevent unrealistically large activity extrapolations in the times between t=0 and the first measurement. By setting the amplitude parameter A_1 equal to the negative sum of the A_2 and A_3 coefficients, the curve will necessarily pass through the origin at the time of administration and a generic k_1 coefficient should be applied which allows uptake to complete prior to the first measurement (typically in the first several hours) but mitigates the potential for large area under the curve in the initial moments post-administration. In this instance, an empirically chosen k_1 value of -1.3 (approximately 30 minutes half-time) appears to provide a reasonable approximation for a variety of tissue types. The results of experiments with other rate parameters for half-times of 20, 60, and 90 minutes are provided in Supplementary Table 1 and yield time-integrated activity values within 2% in all instances, except in tissues with a particularly large component of early-phase clearance such as urinary bladder and heart (blood pool).

[Supplementary Table 1]

Figure Captions:

Figure 1: Decay-correcting initial measured data before fitting ensures algorithm does not fit increasing pharmacological concentration beyond final imaging time point. This is accounted for when calculating time-integrated activity and easily permits estimates from diagnostic/therapeutic isotope pairs such as $^{124}I/^{131}I$.

Figure 2 - Illustration of typical time-activity curve comprised of three exponential phases that has been solved to pass through measured data points. Plots of the component exponential curves, one uptake and two clearance, are shown as dashed lines. The sum of phases 2 & 3 and all phases are shown as shown as solid green and solid blue, respectively. Note that phase 1 and phase 2 effectively deplete as the curve nears measurement time points 1 & 2.

Figure 3 - Standard (left) and logarithmic (right) plots of method to solve late-phase clearance based on exponential slope between measurement time points 2 and 3.

Figure 4 - Method to solve phase 2, first clearance phase, based on the difference in the curve described by Figure 2 and the measured activity at time point 1. Standard (left) and logarithmic (right) plots are shown to illustrate piecewise nature of the individual curve phases.

Supplementary Figure 1: Time-activity curve approximated for data with greatest uptake measured at the final time point c_3. Physical decay is assumed beyond and a single uptake phase may be used to approximate the kinetics between t=0 and c_3. Dotted line represents the late-phase retention beyond c_3. On right plot, separate phases are plotted individually; uptake phase shown as dashed line. The resulting time-activity curve is shown as solid line against measured values on left.

Supplementary Figure 2: Example of serial activity measurements requiring conditional adjustment to solve analytical time-activity curve. This may occur due to image alignment issues or noise and is unlikely to represent true physiology. Here the activity declines at c_2 and increases again at c_3. This may be detected by conditional statement and the measurement c_2 is adjusted to match the slope for very near physical clearance between time-points c_2 and c_3. The piecewise solving process may then proceed as normal.

Supplementary Figure 3: A second pattern of measurement that may be detected by conditional statement. By first shifting the measured activity at c_2 to the linear interpolation between c_1 and c_3, solving with the piecewise algorithm approximates the behaviour of a least-squares optimiser, yielding a curve that is a compromise of early measured data.

Supplementary Figure 4: Initial preconditioning of values with very low measurements relative to the second time point. These tend to occur in low-uptake regions or where there are errors in image alignment and this may prevent calculation of very large exponential decay slopes.

Supplementary Figure 5: Calculation of comparison values $c_{2,plateau}$ and $c_{2, linear}$ which may be employed to handle unrealistic cases (eg. high-low-high uptake).

Supplementary Figure 6 - Primary flow-chart for solving time-activity curve as a two- or three-phase exponential decay curve. Note: the common case with one uptake phase and two separate clearance components is denoted in bold.

Table 1 - Estimated time-integrated activity for representative cohort of ^{177}Lu-DOTA-Octreotate therapies as computed using proposed tri-exponential algorithm, Voxel-based Multimodal, and simplified piecewise with single late-phase exponential methods. Results are provided based on curves computed at the voxel level (mean of all curves) and additionally based on a single curve for each organ using the mean activity concentration at each timepoint.

	Mean Time-Integrated Activity Concentration (MBq*h/ml)					
	Voxel Level:			**Whole Organ:**		
	Tri-exponential	**VoMM**	**Trapezoid + Single Exponential**	**Tri-exponential**	**VoMM**	**Trapezoid + Single Exponential**
Marrow	2.78	2.52	2.95	2.78	2.86	2.88
Muscle	1.21	1.22	1.28	1.03	1.06	1.05
Lung	1.01	1.04	1.11	0.95	0.96	1.04
Heart	1.62	1.71	1.76	1.54	1.62	1.64
Stomach	14.92	13.86	15.57	14.03	13.51	14.39
Small Bowel	3.51	3.32	3.65	2.93	2.97	2.93
Liver	27.46	24.96	27.98	26.53	26.74	26.08
Pancreas	17.53	15.04	18.64	18.02	16.20	19.18
Spleen	56.26	52.05	57.64	53.43	53.82	52.54
Right Kidney	39.27	35.96	40.16	36.97	37.51	36.86
Left Kidney	35.88	32.61	36.38	33.99	34.88	33.98
Bladder	20.23	25.33	34.65	18.99	24.81	33.13
Lower Large Intestine	10.92	7.40	10.85	10.41	7.79	10.28
Upper Large Intestine	5.35	4.96	5.14	4.83	4.22	4.55
Tumor	327.83	290.79	345.99	330.26	347.25	351.85

Table 2 - Median Voxel Level error as relative percentage at each of the three imaging time points. Note that the iterative solving method (VoMM) is biased toward reducing error at early images as when activity and associated calculation of residual error would be greatest. The proposed tri-exponential algorithm prioritizes accuracy for the second and third measurements with consideration of the late phase influence on the estimated time integral.

	4h		24h		72h	
Region	Tri-exponential	VoMM	Tri-exponential	VoMM	Tri-exponential	VoMM
Marrow	5.0%	1.4%	10.3%	7.4%	0.0%	12.2%
Muscle	3.8%	0.5%	8.2%	3.9%	0.0%	11.7%
Lung	8.4%	0.1%	5.7%	1.2%	0.0%	9.3%
Heart	5.5%	0.1%	4.9%	1.1%	0.0%	9.2%
Stomach	8.5%	4.7%	6.3%	7.2%	0.2%	7.1%
Small Bowel	12.5%	1.9%	7.6%	7.5%	0.2%	14.8%
Liver	3.2%	0.4%	1.9%	1.4%	0.1%	2.5%
Pancreas	5.7%	4.5%	12.1%	7.2%	0.1%	7.9%
Spleen	4.2%	1.1%	2.8%	3.4%	0.1%	6.2%
Right Kidney	4.3%	0.5%	1.3%	2.3%	0.1%	13.8%
Left Kidney	4.2%	0.6%	1.6%	2.7%	0.0%	14.6%
Bladder	7.2%	0.0%	1.9%	0.6%	0.0%	51.2%
Lower Large Intestine	77.0%	13.7%	3.6%	13.4%	0.1%	10.0%
Upper Large Intestine	21.4%	5.9%	2.2%	8.0%	0.2%	16.7%
Tumor	15.9%	4.7%	8.5%	7.3%	0.3%	15.2%

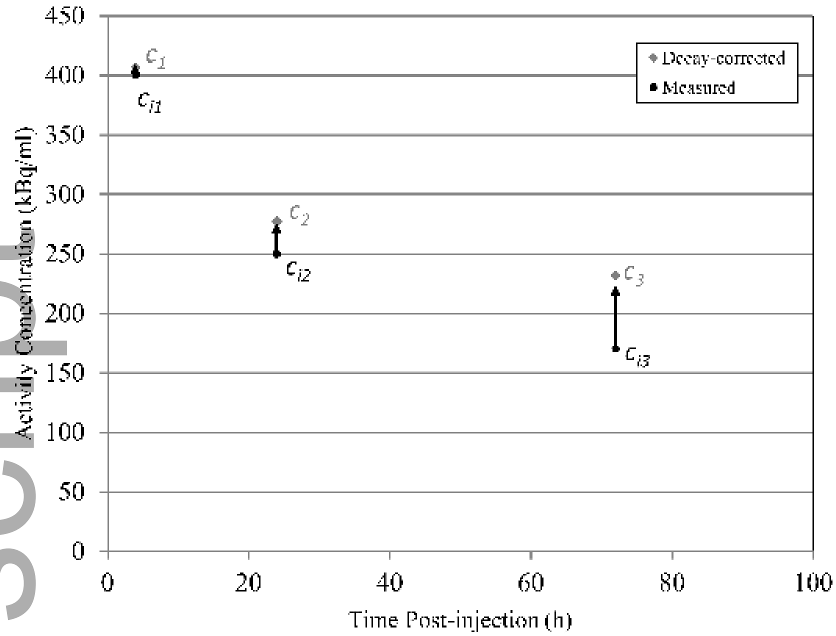

mp_14243_f1.jpg

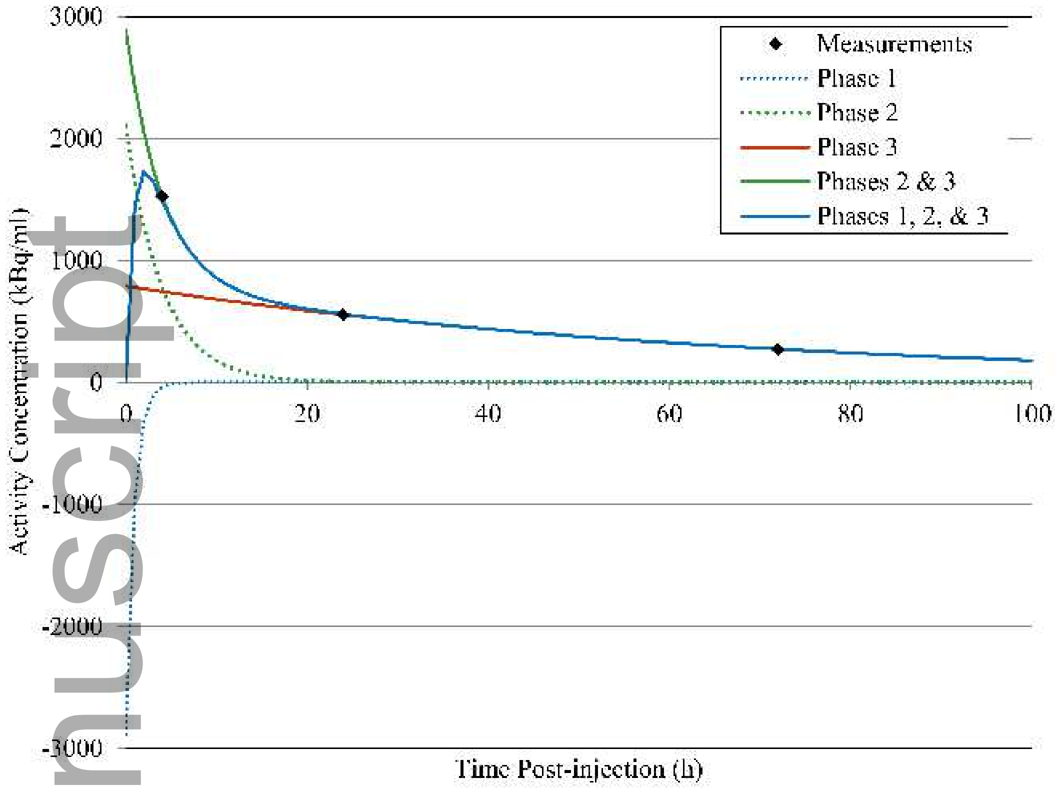

mp_14243_f2.jpg

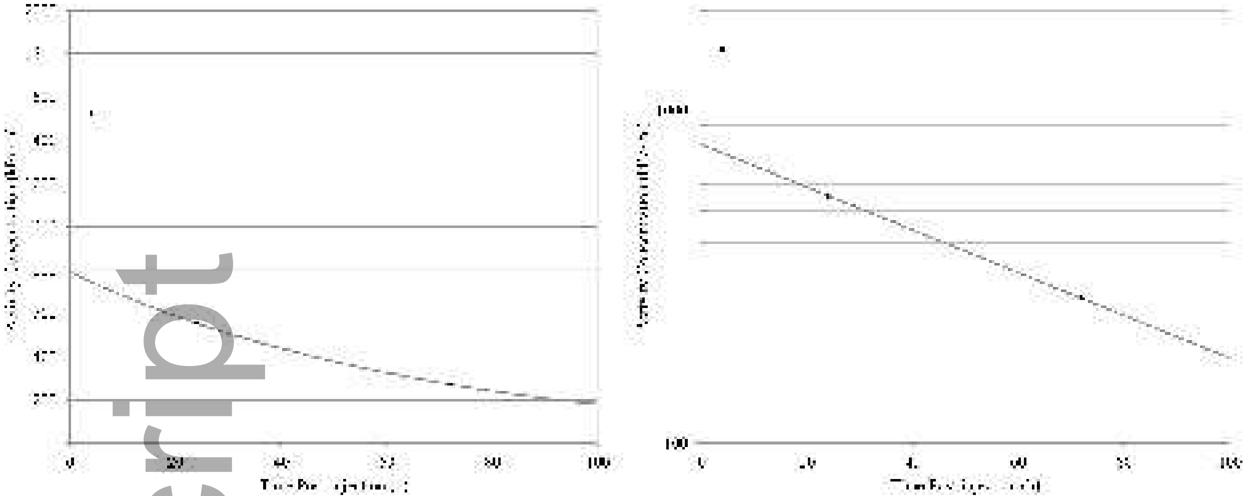

mp_14243_f3.jpg

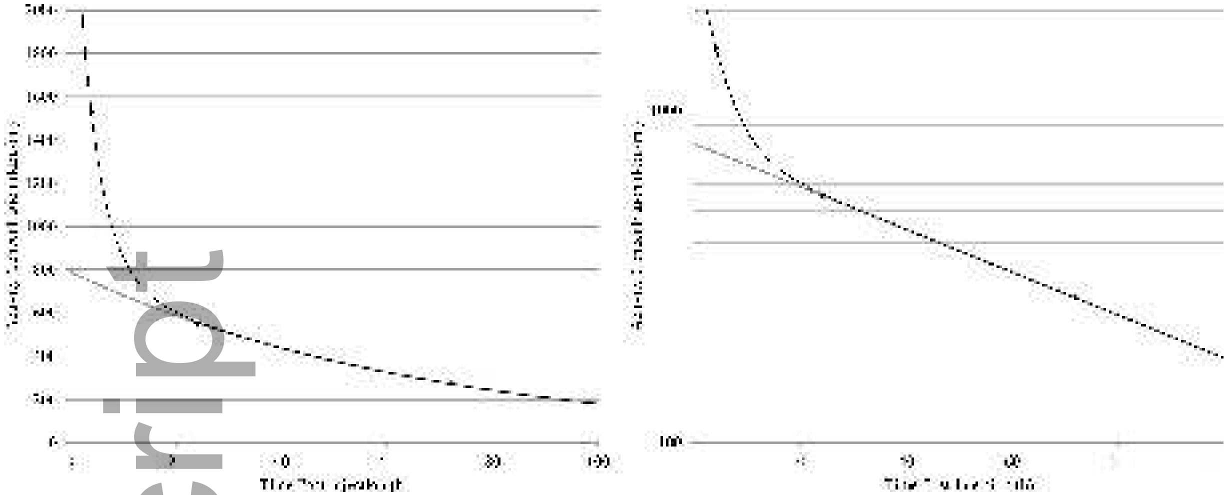

mp_14243_f4.jpg